

## Producing swimmers by coupling reaction-diffusion equations to a chemically responsive material

C. M. Pooley<sup>1,\*</sup> and Anna C. Balazs<sup>2</sup><sup>1</sup>*Rudolf Peierls Centre for Theoretical Physics, 1 Keble Road, Oxford, OX1 3NP, United Kingdom*<sup>2</sup>*Chemical Engineering Department, University of Pittsburgh, 1249 Benedum Hall, Pittsburgh, Pennsylvania 15261, USA*

(Received 5 May 2006; revised manuscript received 8 January 2007; published 18 July 2007)

We propose a mechanism for generating snakelike motion in a micrometer-scale, responsive, synthetic material, which thereby undergoes net movement in a fluid (i.e., swimming). By responsive material, we refer to a material that can expand or contract in response to a chemical concentration change. The concentrations of the chemical species are modeled by simple reaction-diffusion equations with suitably chosen source terms. Using linear stability analysis, we isolate the key properties of the material and reaction rate parameters.

DOI: 10.1103/PhysRevE.76.016308

PACS number(s): 47.63.Gd, 82.20.-w, 47.63.mf, 47.63.M-

## I. INTRODUCTION

Recently, much attention has been paid to locomotion at low Reynolds number [1], or, in other words, “swimming” at the micrometer scale. This is of importance not only for understanding how biological microorganisms move, but also for designing synthetic materials that can undergo active or self-propelled motion within a fluid. A number of studies have enhanced our understanding of how micrometer-scale objects can achieve movement through periodic distortions in their shape. For instance, Najafi and Golestanian [2] developed a method (proposed earlier by Purcell [3]) in which three spheres are coupled together in a line, and the distances between them are varied in a periodic, nonreciprocal manner to produce motion. Furthermore, Stone and Samuel [4] examined how the velocity of surface distortions can be related to a microorganism’s speed, and Avron *et al.* [5] used conformal mapping techniques to determine optimal solutions for a particular class of two-dimensional swimmers. (In this context, “swimmer” refers to an object that can achieve movement through a periodic change in its shape.)

In 2005, Dreyfus *et al.* [6] constructed the first man-made microscopic swimmers. These consisted of a microscopic filament, made up of linked superparamagnetic colloids, with a red blood cell attached at one end. By actuating the device with an external magnetic field, the researchers could produce distorting waves that propagated down the filament length and thus drive the system to swim. At present, no experimental swimmer has been made whose deformation results from internally generated stresses. One of the difficulties lies in the fact that making mechanical devices on the micrometer scale is not easy due to the tiny sizes involved. In this paper, we propose a swimming device that is mechanically very simple, at the expense of introducing some chemical complexity. In particular, the swimming mechanism couples reaction-diffusion equations to a responsive material to induce the required swimming shape changes.

The model we use for the chemistry is generic (see, for example, Ref. [7]). Oscillatory biochemical reactions form the basis for numerous physiological processes [8,9]. There has been remarkable progress achieved during the last two

decades in understanding the general mechanisms of oscillatory chemical reactions. For instance, Esptein *et al.* [10] discuss various pathways to synthesis of chemical oscillations that obey specific requirements. This paper proposes a swimming mechanism that couples a special type of oscillatory chemical wave with a responsive material to induce the required swimming shape changes.

In order to explain this more clearly, we point to the main result, shown in Fig. 1. This depicts the motion of a long, thin piece of a responsive material performing periodic deformations in its shape. The material itself is permeable to the surrounding fluid, and a number of chemical species exist within the system. Two processes act to alter the chemical concentrations as a function of time within the material: reactions between chemicals and diffusion. Together, these processes can give rise to a spatially nonuniform, dynamically changing chemical concentration profile. This is illustrated in Fig. 1 by the shading within the material, which represents the variation in one chemical component, denoted by  $c_a$ . The material locally expands or contracts in response to variation in  $c_a$ , and this produces deformations in its shape. (An example of such a material is a chemoresponsive hydrogel [11].) When coupled to the surrounding fluid, these deformations result in net motion along a specific direction, i.e., from left to right in this example. The motion is similar to that of an eel or snake moving in water, and, by analogy,

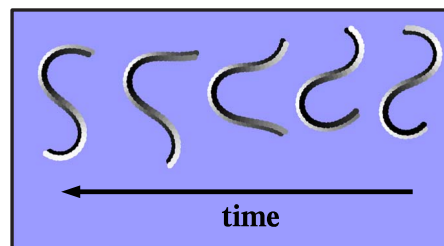


FIG. 1. (Color online) Time evolution of the material shape over half a periodic cycle. A wave propagates in time down the snake body from bottom to top, and this propels the snake downward (note that the last frame is displaced below the first). The shading within the snake indicates the concentration profile  $c_a$ . Since the material is responsive to this chemical, then bright areas denote expanded material and dark areas contracted material. Note that the chemical waves on either side of the snake have opposite phases. We refer to this motion as the swimmer solution.

\*pooley@thphys.ox.ac.uk

we will refer to this piece of material as a snake. The chemical composition of the surrounding fluid provides the constituents to sustain the chemical reactions within the material. In this way, the potential chemical energy is transferred into the kinetic energy necessary to make the snake move.

The paper is arranged in the following order. In Sec. II, we describe the model that is used to describe the dynamical evolution of the chemical concentrations within the responsive material. The numerical simulation results obtained from this model are outlined in Sec. III. By using linear stability analysis, we determine the necessary properties for the material and the chemical reactions to generate swimming motion. Finally, in Sec. IV, we summarize our findings.

## II. MODEL

In this paper, we do not explicitly model the movement of the snake. It has been previously demonstrated that sinusoidal wave propagation down a filament leads to swimming motion [13]. To generate this shape change in a responsive material, it is necessary to induce a chemical distribution similar to that depicted in Fig. 1. That is, the chemical concentration of  $c_a$  varies periodically down the snake and is high on one side of the snake and low on the other side, causing the material to bend. The focus of this work is to determine how such a time-varying chemical distribution can be obtained.

The dynamics of the chemical concentrations are given by

$$\frac{dc_\alpha}{dt} = D_\alpha^s \frac{d^2 c_\alpha}{ds^2} + D_\alpha^p \frac{d^2 c_\alpha}{dp^2} + S_\alpha, \quad (1)$$

where we have introduced the coordinates  $s$  and  $p$ , which are defined to be the distance along and across the snake, respectively. In general, we assume that the diffusion rate along the snake,  $D_\alpha^s$ , is not necessarily the same as that across it,  $D_\alpha^p$ . Later, we show that this is a key feature for the formation of the swimming snake solutions.

We assume that the system contains four chemical species. The source terms in Eq. (1) are written as

$$S_a = f\{-c_b + Bc_a[R^2 - (c_a^2 + c_b^2)] - Ac_c\}, \quad (2)$$

$$S_b = f\{c_a + Bc_b[R^2 - (c_a^2 + c_b^2)] - Ac_d\}, \quad (3)$$

$$S_c = \lambda(c_a - c_c), \quad (4)$$

$$S_d = \lambda(c_b - c_d). \quad (5)$$

These equations are constructed from a number of necessary pieces. The first terms inside the curly brackets in Eqs. (2) and (3) result in an oscillatory reaction between the  $c_a$  and  $c_b$  chemical species. This corresponds to circular trajectories on the phase portrait in the  $c_a/c_b$  plane. The second terms in the curly brackets (containing the parameter  $B$ ) ensure that all trajectories converge onto a single circular curve, which is a stable limit-cycle attractor of radius  $R$ . Figure 2 shows the phase portrait arising from these two terms. The origin in Fig. 2 is taken to be the natural concentration of chemical species when no reactions are taking place; hence, negative

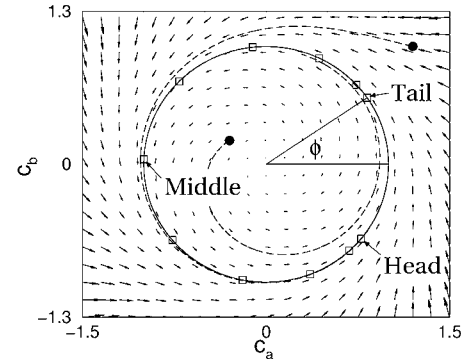


FIG. 2. Phase portrait in the  $c_d/c_b$  plane for Eq. (1) (while neglecting diffusion), using the source terms in Eqs. (2)–(5). The black dots show two initial conditions, and the dashed lines show how these trajectories converge onto a single, stable limit-cycle attractor, denoted by the solid line. The squares show the relative phases of 11 different points in the snake, ordered from head to tail, for the long-wavelength solution. The stable limit cycle has a radius of  $R$ .

values of  $c_\alpha$  do not correspond to unphysical, negative concentrations.

The parameter  $f$  in Eqs. (2) and (3) introduces an asymmetry in the system that dictates the direction in which the snake moves. We take  $f$  to have a simple linear profile in the  $s$  direction.

$$f = \bar{f} + \frac{df}{ds}s, \quad (6)$$

where  $\bar{f}$  and  $df/ds$  are both constants. We chose  $(df/ds)L \ll \bar{f}$ , where  $L$  is the length of the snake, such that the value of  $f$  is only slightly higher at the head of the snake than that at the tail (typically  $\sim 2\%$  in the simulations). The factor  $f$  can be interpreted in a number of ways. It can, for example, be thought of as a chemical gradient in the surrounding fluid that helps to catalyze the reactions, or as a temperature differential between the head and tail of the snake. In any case, this gradient is introduced or initiated through some external conditions.

In the absence of diffusion,  $f$  is the angular frequency of oscillations around the limit cycle (that is, the frequency of the chemical oscillations in the system). Since we define  $f$  to have a small, positive gradient in the  $s$  direction, then the “head” will tend to naturally (that is, without diffusion) oscillate at a slightly higher frequency than the “tail.” However, diffusion acts to couple all parts of the snake, such that they oscillate at the *same* frequency  $\bar{f}$  [14], and not  $f$ . The discrepancy between  $f$  and  $\bar{f}$  results in different regions of the snake having different phases  $\phi$ . This is represented by the squares in Fig. 2, which give a snapshot in time of the chemical composition of 11 points in the snake, ordered in equally spaced intervals from head to tail. [These results were obtained by numerically solving Eq. (1), as described later.] In this example, the chemical concentration  $c_a$  is around 0.8 at the head, drops to  $-1$  in the middle, and goes back up to 0.8 at the tail. In other words, it has a wave profile

going down the snake body. In time, this wave propagates from the head to the tail. (It has been previously pointed out that the oscillator with the highest frequency entrains others with which it interacts [12].)

The above discussion has shown that the first two terms in Eqs. (2) and (3) can produce long-wavelength chemical waves propagating down the snake [when solving Eq. (1)]. This is, however, not what is required for swimming. The pictures in Fig. 1 show that it is also necessary for the phase of the wave on one edge to be opposite to that on the other. It is this behavior that causes the snake to bend and, consequently, undergo net movement. For this reason, the last terms in Eqs. (2) and (3), and the chemical species  $c_c$  and  $c_d$ , are introduced. As will become apparent below, these terms suppress the solutions that are independent of  $p$ , thus allowing the appearance of the required swimming behavior.

### III. RESULTS

The dynamic equations (1) are solved using a finite difference method on a square grid of lattice size  $L_s=100$  and  $L_p=5$ . In the following analysis, we neglect the effects of distortions in the snake shape on the diffusion constants. We use a no-flux boundary condition on the snake edges ( $dc_\alpha/ds=dc_\alpha/dp=0$ ). This scenario can be interpreted as the snake being coated in a semipermeable membrane. This membrane would allow small molecular weight molecules, such as water, and a chemical energy supply to enter and leave, but block the flux of the active chemical species  $c_\alpha$ , which we assume to be larger than the pore size.

For simplicity, we assume that the diffusive constants obey  $D_a^s=D_b^s=D_{a,b}^s$ ,  $D_a^p=D_b^p=D_{a,b}^p$ ,  $D_c^s=D_d^s=D_{c,d}^s$ , and  $D_c^p=D_d^p=D_{c,d}^p$ , such that the model is symmetric between the  $a$  and  $b$  species, and between the  $c$  and  $d$  species. Initially, the chemical concentrations are set to  $c_\alpha=1$  plus a small random perturbation. The system is dynamically evolved for  $10^5$  time steps of size  $\Delta t=0.005$  [by numerically integrating Eq. (1)], allowing the long-time behavior to be measured. By varying the parameters in the model, we find that the system exhibits five different types of behavior, two of which result in swimming motion. The details of each of these are described below.

The first, shown in Fig. 3(a), represents the fixed point solution  $c_a=c_b=c_c=c_d=0$ . This corresponds to a constant chemical concentration in the system, and thus the snake does not move. In all of the diagrams in Fig. 3, the shading represents the concentration of  $c_a$  across the system. Since the stable limit cycle is a loop of radius  $R$  in the phase portrait Fig. 2, then  $c_a$  varies between  $c_a=R$  and  $-R$ . Thus, we choose white areas in Fig. 3 to represent  $c_a=R$ , and black areas to represent  $c_a=-R$ .

The second solution is a long-wavelength wave that propagates in the negative  $s$  direction, and is constant in the  $p$  direction. Figure 3(b) shows the time evolution of this wave over one cycle. By observing these patterns, we can use a combination of deduction and trial and error to obtain (for small amplitudes) the functional form of this solution as

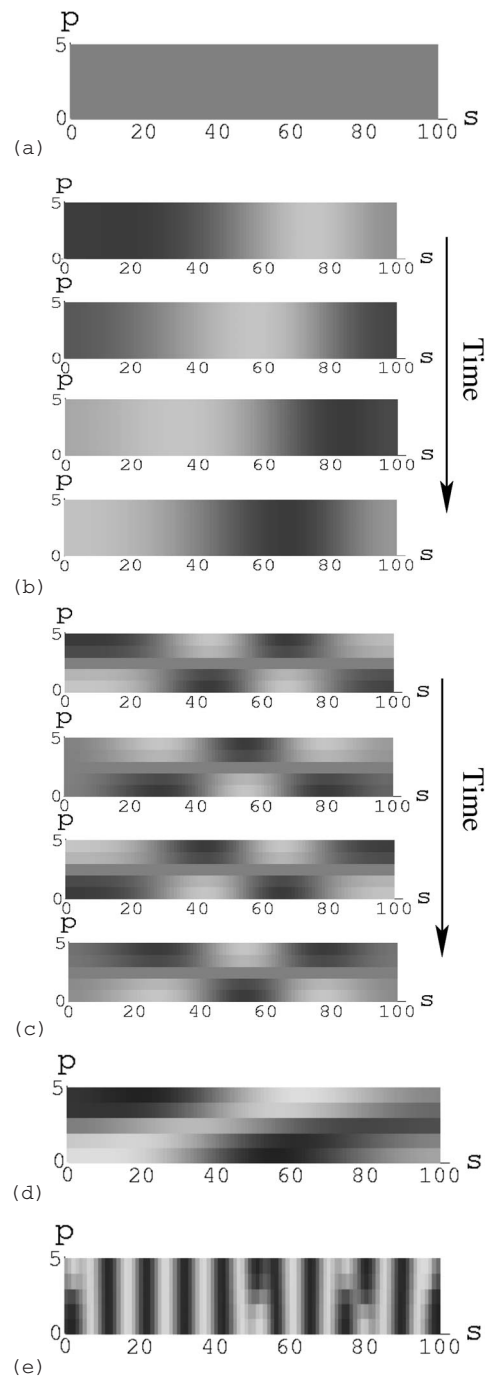


FIG. 3. Density of chemical species  $c_a$  as a function of  $s$ , the distance down the snake, and  $p$ , the distance across the snake. Bright areas represent  $c_a=R$ , and dark areas  $c_a=-R$ . Note that the  $p$  axis has been elongated to enhance clarity. (a) The fixed point solution. Here, the chemical concentration is constant,  $c_a=0$ , and was generated using the parameters  $A=3$ ,  $B=2$ ,  $\lambda=6$ ,  $D_{c,d}^s=1$ , and  $D_{c,d}^p=5$ . (b) The time evolution of the long-wavelength solution as one wave propagates down the snake body ( $A=3$ ,  $B=2$ ,  $\lambda=2$ ,  $D_{c,d}^s=1$ , and  $D_{c,d}^p=5$ ). (c) The time evolution of the swimmer solution as one wave propagates down the snake body ( $A=3$ ,  $B=2$ ,  $\lambda=4$ ,  $D_{c,d}^s=1$ , and  $D_{c,d}^p=25$ ). (d) A snapshot of the partial swimmer solution ( $A=3$ ,  $B=3$ ,  $\lambda=2$ ,  $D_{c,d}^s=1$  and  $D_{c,d}^p=25$ ). (e) A snapshot of the short-wavelength solution ( $A=3$ ,  $B=3$ ,  $\lambda=2$ ,  $D_{c,d}^s=25$ , and  $D_{c,d}^p=25$ ).

$$c_a = \delta \cos(\bar{f}t + \phi),$$

$$c_b = \delta \sin(\bar{f}t + \phi),$$

$$c_c = \delta' \cos(\bar{f}t + \phi) + \delta' \sin(\bar{f}t + \phi),$$

$$c_d = \delta' \sin(\bar{f}t + \phi) - \delta' \cos(\bar{f}t + \phi), \quad (7)$$

where the phase angle is given by

$$\phi = \frac{1}{2D_{a,b}^s} \frac{df}{ds} \left[ \left( \frac{L}{2} \right)^2 s - \frac{s^3}{3} \right]. \quad (8)$$

Expressions for  $\delta'$  and  $\delta''$  are obtained by substituting these equations into Eq. (1), and using the source terms in Eqs. (2)–(5). For instance, the separate cosine and sine parts of the time evolution equation for the component  $c_c$  become

$$\frac{d\delta'}{dt} + \bar{f}\delta' = \left[ - \left( \frac{d\phi}{ds} \right)^2 \delta' + \frac{d^2\phi}{ds^2} \delta' \right] D_{c,d}^s + \lambda(\delta - \delta'), \quad (9)$$

$$-\bar{f}\delta'' = - \left[ \frac{d^2\phi}{ds^2} \delta' + \left( \frac{d\phi}{ds} \right)^2 \delta' \right] D_{c,d}^s - \lambda\delta'. \quad (10)$$

The first term on the right-hand side of Eq. (10) can be neglected because of the condition  $(df/ds)L \ll \bar{f}$  stated earlier [see Eq. (6)]. To proceed further, it is necessary to assume that the second term is also small, which leads to the constraint

$$\left( \frac{L^2 df}{8 ds} \right)^2 \frac{D_{c,d}^s}{D_{a,b}^{s^2}} \ll \lambda. \quad (11)$$

This states, to a first approximation, that it is possible to neglect diffusion in the  $s$  direction. This is intuitively clear, because diffusion over long distances down the body of the filament is very slow compared to the chemical relaxation time scale  $\lambda^{-1}$ . With these approximations, Eq. (10) becomes  $\delta'' = \delta' \bar{f} / \lambda$ . We assume the case when  $\lambda \gg \bar{f}$ , and thus  $\delta''$  is a small quantity, and terms containing this are subsequently neglected.

In linear stability analysis, we are interested in states that are near the critical point, so their chemical amplitudes are either growing or shrinking very slowly. Thus, the first term on the left-hand side of Eq. (9) can be ignored. The first term on the right-hand side is also small, because of the condition Eq. (11), leaving  $\delta' = \delta$ . In this regime the chemical concentration of  $c_c$  is strongly coupled to follow  $c_a$ .

An analysis of the cosine and sine parts of the time evolution equation for  $c_a$  gives

$$\frac{d\delta}{dt} = - \left( \frac{d\phi}{ds} \right)^2 \delta D_{a,b}^s + \left( \bar{f} + \frac{df}{ds} s \right) (BR^2 - A) \delta, \quad (12)$$

$$-\bar{f}\delta = - \frac{d^2\phi}{ds^2} \delta D_{a,b}^s - \left( \bar{f} + \frac{df}{ds} s \right) \delta, \quad (13)$$

where the  $\delta''$  terms have been ignored. Substitution of Eq. (8) into Eq. (13) shows that this equality is true. Assuming that

the first term on the right-hand side of Eq. (12) is small, then

$$\left( \frac{L^2 df}{8 ds} \right)^2 \frac{1}{D_{a,b}^s} \ll \bar{f}, \quad (14)$$

which is a stricter condition than (11), now stating that diffusion times must be much slower than the oscillation period of the chemicals. This leaves the time evolution of the perturbation amplitude given by

$$\frac{d\delta}{dt} = \Gamma \delta, \quad (15)$$

where the growth rate is

$$\Gamma = \bar{f}(BR^2 - A). \quad (16)$$

Note that the phase of the wave  $\phi$  [see Eq. (8)] does not change linearly down the snake. Rather,  $d\phi/ds$  follows a parabolic path, which is zero at the ends ( $s = \pm L/2$ ) and at a maximum in the middle ( $s=0$ ). This can be seen clearly in Fig. 2, by virtue of the fact that the squares are more spaced out in the middle of the snake than at the head or the tail.

The third solution, depicted in Fig. 3(c), is that required for swimming motion. When this concentration profile is coupled to a responsive material it induces the conformational change illustrated in Fig. 1, i.e., it generates snakelike distortions. Again, through deduction and trial and error, we find that the chemical behavior can be described by the following equations:

$$c_a = \delta \cos(\bar{f}t + \phi) \sin(k_p p),$$

$$c_b = \delta \sin(\bar{f}t + \phi) \sin(k_p p),$$

$$c_c = [\delta' \cos(\bar{f}t + \phi) + \delta' \sin(\bar{f}t + \phi)] \sin(k_p p),$$

$$c_d = [\delta' \sin(\bar{f}t + \phi) - \delta' \cos(\bar{f}t + \phi)] \sin(k_p p), \quad (17)$$

where  $k_p = \pi/W$  and  $W$  is the width of the snake. This is the same as solution number 2 [Eq. (7)], with the exception of containing a final multiplicative sine term. This changes  $\delta'$  and  $\delta''$ , to now give

$$\delta' = \frac{\delta}{1 + k_p^2 D_{c,d}^p / \lambda},$$

$$\delta'' = \frac{\delta' \bar{f}}{\lambda + D_{c,d}^p k_p^2}, \quad (18)$$

with a growth rate [see Eq. (15)]

$$\Gamma = -D_{a,b}^p k_p^2 + \bar{f} \left( BR^2 - \frac{A}{1 + D_{c,d}^p k_p^2 / \lambda} \right). \quad (19)$$

The fourth solution is termed the partial swimmer solution, as it does result in swimming motion, but it is less efficient. A snapshot is show in Fig. 3(d). It is characterized by its asymmetric nature; regions of alternating high and low concentration of  $c_a$  link diagonally across the body. This can

be thought of as an intermediate between solutions 2 and 3. It was not possible to obtain a small-amplitude solution for this behavior.

Finally, the fifth solution consists of waves of short wavelength, moving parallel to the snake axis  $s$  in *both* directions. This is illustrated in Fig. 3(e). In the regions  $s=0-50$  and  $s=80-9$ , the waves travel right, and in the range  $s=50-80$ , they travel left. As these waves collide, we see defects. Also, the waves are distorted at the end points to accommodate the boundary conditions. Mathematically, they are described by

$$c_a = \delta \cos(\bar{f}t \pm k_s s),$$

$$c_b = \delta \sin(\bar{f}t \pm k_s s),$$

$$c_c = \delta' \cos(\bar{f}t \pm k_s s) + \delta'' \sin(\bar{f}t \pm k_s s),$$

$$c_d = \delta' \sin(\bar{f}t \pm k_s s) - \delta'' \cos(\bar{f}t \pm k_s s). \quad (20)$$

By substitution, we find this is a solution of Eq. (1), with  $k_s$  replacing  $k_p$ , and  $D_{c,d}^s$  replacing  $D_{c,d}^p$  in Eq. (18). The growth rate in this case is given by

$$\Gamma = -D_{a,b}^s k_s^2 + \bar{f} \left( BR^2 - \frac{A}{1 + D_{c,d}^s k_s^2 / \lambda} \right). \quad (21)$$

Note that the value of  $k_s$  is not specified. In other words, Eq. (20) is a solution for arbitrary wave number. In the linear stability analysis below, we numerically calculate the value of  $k_s$  that maximizes  $\Gamma$ .

To understand under what circumstances each of these five solutions is selected by the system, we construct the phase diagrams shown in Figs. 4–6 (which are obtained numerically, as described below). For instance, Fig. 4 shows the effect of varying the parameters  $A$  and  $B$ , while keeping all others fixed ( $\lambda=2$ ,  $D_{c,d}^s=1$ , and  $D_{c,d}^p=25$ ). In all the diagrams we set  $D_{a,b}^s=D_{a,b}^p=1$  and  $R=1$ . Each of these diagrams is divided into a grid of  $80 \times 60$  points. At each of these points, the dynamic equations [Eq. (1) using the source term in Eqs. (2)–(5)] are integrated until the long-time behavior is achieved (in exactly the same way as for Fig. 3). Then the time average of the trajectory radius, defined to be  $\bar{r} = \langle \sqrt{(c_a^2 + c_b^2)} \rangle_t$ , is measured in two places: one in the middle of the snake, at position  $(L/2, W/2)$ , and the other on the side of the snake, at position  $(L/2, 0)$ . Note that  $\bar{r}$  is a measure of the magnitude of chemical oscillations in the system. The results are shown in Figs. 4(a) and 4(b), respectively. Black shading represents a time average of zero, and white represents a time average of  $R$ .

Using these two diagrams, it is possible to identify different regimes of behavior. For example, the fixed point solution clearly has a time average of zero, so it is black in both diagrams. For the swimmer solution in Eq. (17),  $\bar{r}$  is high on the lateral edge of the snake. This is indicated by the fact that the point  $s=50, p=0$  in Fig. 3(c) exhibits large oscillations in concentration of  $c_a$  in time (correspondingly  $c_b$  also oscillates). However, this figure also shows that in the center of the snake, at the point  $s=50, p=2.5$ ,  $c_a$  is zero (as is  $c_b$ ), and hence  $\bar{r}=0$ . These two properties are reflected in the phase

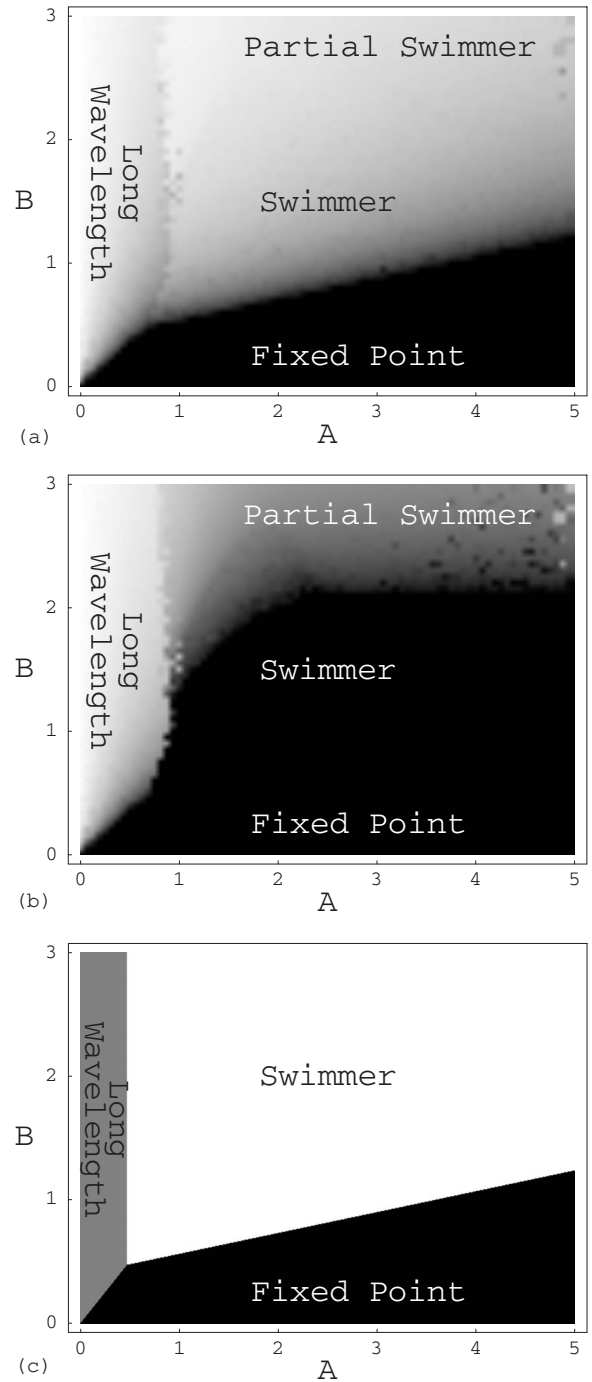


FIG. 4. Phase diagrams in the  $A$ - $B$  plane, using the fixed parameters  $\lambda=2$ ,  $D_{a,b}^p=D_{a,b}^s=D_{c,d}^s=1$ , and  $D_{c,d}^p=25$ . The shading indicates the time average of the trajectory radius,  $\langle \sqrt{(c_a^2 + c_b^2)} \rangle_t$ , (a) at the middle of the snake at point  $(L/2, W/2)$ , and (b) on the side of the snake at point  $(L/2, 0)$ . (c) The phase diagram based on simple linear stability analysis.

diagrams by the point corresponding to the particular choice of system parameters ( $A=3$  and  $B=2$ ) being light in Fig. 4(a), and dark in Fig. 4(b).

Figure 4(c) shows the result of linear stability analysis. This is found by calculating which of the growth rates [Eqs. (16), (19), and (21), or  $\Gamma=0$  for the fixed point] is largest for

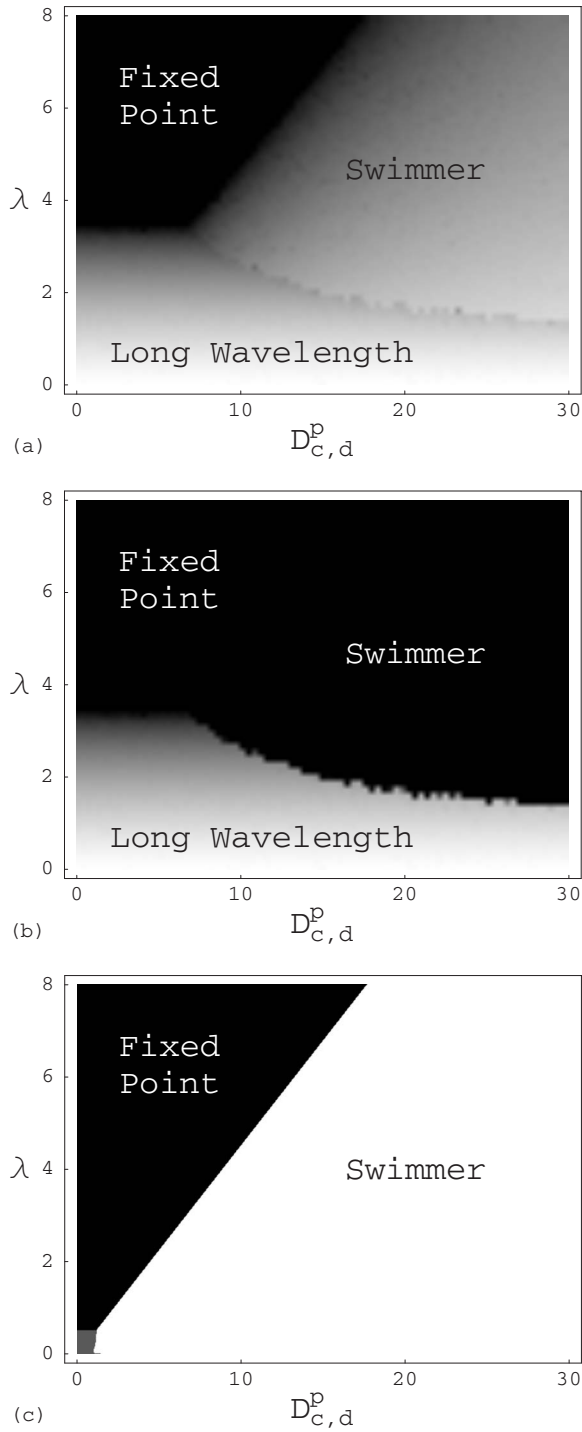


FIG. 5. Phase diagrams in the  $D_{c,d}^p$ - $\lambda$  plane, using the fixed parameters  $A=3$ ,  $B=2$ , and  $D_{a,b}^p=D_{a,b}^s=D_{c,d}^s=1$ . The shading indicates the time average of the trajectory radius,  $\langle \sqrt{(c_a^2+c_b^2)} \rangle_t$ , (a) at the middle of the snake at point  $(L/2, W/2)$ , and (b) on the side of the snake at point  $(L/2, 0)$ . (c) The phase diagram based on simple linear stability analysis.

a given parameter set. This method gives exact boundaries for the onset of an instability (e.g., between the fixed point and swimmer or long-wavelength regions) and approximated boundaries between two growing solutions (e.g., between the swimmer and long-wavelength areas). By comparing Fig.

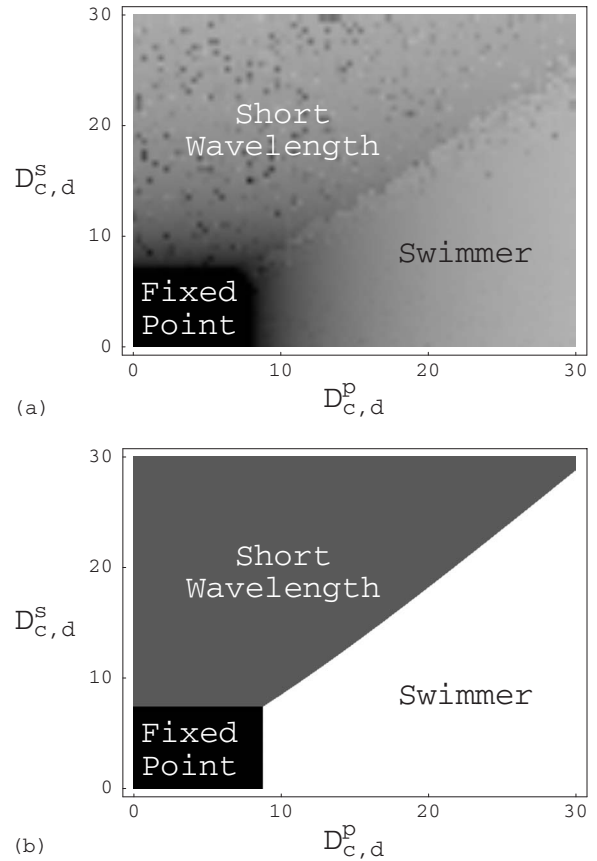


FIG. 6. Phase diagram in the  $D_{c,d}^p$ - $D_{c,d}^s$  plane, using the fixed parameters  $A=3$ ,  $B=2$ ,  $\lambda=4$ , and  $D_{a,b}^p=D_{a,b}^s=1$ . (a) The shading indicates the time average of the trajectory radius,  $\langle \sqrt{(c_a^2+c_b^2)} \rangle_t$ , on the side of the snake at point  $(L/2, 0)$ . (b) The phase diagram based on simple linear stability analysis.

4(c) with Figs. 4(a) and 4(b), we find that the linear stability analysis can qualitatively describe the regions in the diagram in which we observe fixed point, long-wavelength, and swimmer motion. Note that we could not obtain an analytical expression for the behavior of the partial swimmer; hence this does not appear in Fig. 4(c).

The role of  $c_c$  and  $c_d$ , can be interpreted in a simplified way. In the absence of diffusion, Eq. (1), with source term Eq. (4), tends to change  $c_c$  such that it approaches  $c_c=c_a$ , on a time scale given by  $\lambda^{-1}$ . However, the effect of diffusion is to smooth out any variation in concentration. Specifically, this averaging effect is over a length scale given by  $\sqrt{D_{c,d}^{s,p}/\lambda}$ . In other words, what  $c_c$  actually represents is the average of  $c_a$  over an approximate ellipsoidal region, with principle radii in the  $s$  and  $p$  directions given by  $\sqrt{D_{c,d}^s/\lambda}$  and  $\sqrt{D_{c,d}^p/\lambda}$ , respectively. For the swimmer solution to exist,  $D_{c,d}^p$  has to be significantly larger than  $D_{c,d}^s$  (this will become more apparent later when we analyze Fig. 6). For example,  $D_{c,d}^p=25$  and  $D_{c,d}^s=1$  in Fig. 4. This means that the averaging is predominantly in the  $p$  direction. If  $\sqrt{D_{c,d}^p/\lambda} \geq W$ , as in Fig. 4, then  $c_c$  can be thought of simply as the average of  $c_a$  across the snake in the  $p$  direction,  $c_c \approx \langle c_a \rangle_p$ . If we consider the swimmer solution [Eq. (17)], then we find  $c_{c,d} \approx \langle c_{a,b} \rangle_p \approx 0$  (although not exactly zero), so the  $A$  terms in Eqs. (2)

and (3) have little effect. However, for the long-wavelength solutions [Eq. (7)], we find  $c_c \approx c_a$  and  $c_d \approx c_b$ ; hence, the  $A$  term now acts against the  $B$  term to reduce the radius of the trajectories, and, if sufficiently large, removes the stable limit cycle altogether. Put simply, the  $A$  term destabilizes the long-wavelength solution with respect to the swimmer solution, allowing the swimmer solution to be the one actually observed.

Figure 5 shows the corresponding diagrams for varying  $\lambda$  and  $D_{c,d}^p$ , while keeping  $A=3$ ,  $B=2$ , and  $D_{c,d}^s=1$  fixed. No swimmer solution exists for  $D_{c,d}^p \lesssim 8$  [this can be most clearly seen in Fig. 5(a), in which the swimmer region does not extend below  $D_{c,d}^p=8$ ]. This reflects a more general feature of these equations, which is the requirement that  $D_{c,d}^p \gg D_{a,b}^p$  for swimmer solutions to exist (recall that  $D_{a,b}^p=1$ ).

If  $\lambda \ll \bar{f}$ , then the values of  $c_c$  and  $c_d$  change so slowly that they no longer track the values of  $c_a$  and  $c_b$ , and tend to get averaged out to zero in time. In this limit, the long-wavelength solutions are no longer unstable, and so they can be observed on the lower part of the diagram in Fig. 5(a). On the other hand, if  $\lambda$  is very large, then the condition  $\sqrt{D_{c,d}^p}/\lambda \gtrsim W$ , necessary for the swimmer solutions to exist, is violated. This condition can be rearranged into the form  $D_{c,d}^p \gtrsim W^2\lambda$ , which is represented in Fig. 5(a) by the line dividing the swimmer and fixed point regions.

Figure 5(c) shows the result of linear stability analysis. [As before, this is found by calculating which of the growth rates, Eqs. (16), (19), and (21) or  $\Gamma=0$  for the fixed point, is largest.] We note that, although it does capture the qualitative shape of the phase diagram correctly, there is a significant discrepancy when compared to the numerical results in Figs. 5(a) and 5(b). This difference reflects the nonlinear nature of the actual solutions observed, and the violation of assumptions used in deriving the analytic results. (In particular, the condition  $\lambda \gg \bar{f}$  is violated as  $\lambda$  becomes small.)

Figure 6(a) shows how the system's behavior depends on the diffusion of the  $c_{c,d}$  components along the snake axis,

$D_{c,d}^s$ , and perpendicular to the snake axis,  $D_{c,d}^p$ . There are two important points to be made. First, the diffusion in the perpendicular direction must be at least eight times that of the two oscillatory components (in this example  $D_{a,b}^p=1$ ). Below this value, the system approaches the fixed point in the bottom left-hand corner of the diagram. Second, the diffusion in the perpendicular direction for the  $c$  and  $d$  components has to be always larger than that in the parallel direction. That is, the line  $D_{c,d}^s=D_{c,d}^p$  on the phase diagram always passes through the nonswimming, short-wavelength solution. For completeness, we include the linear stability diagram in Fig. 6(b), which shows good agreement with Fig. 6(a).

#### IV. SUMMARY

To summarize, we have demonstrated that it is possible to obtain swimmers, such as that illustrated in Fig. 1, by coupling reaction-diffusion equations to a chemically responsive material. We suggest a simple model, and obtain a number of constraints on the system parameters. First, two of the chemical components must form an oscillatory reaction (see Fig. 2). The oscillation period must be fast in order for rapid swimming. Second, the frequency of oscillations must be slightly higher at the head of the snake than that at the tail. This determines the direction of swimming. Third, there must exist one, or more, other components that suppress the chemical oscillations [this role was played by  $c_c$  and  $c_d$  in Eqs. (2) and (3)]. These components must have a much higher diffusion rate (as illustrated in Fig. 5), and preferentially diffuse in the direction perpendicular to the snake axis (shown in Fig. 6).

#### ACKNOWLEDGMENTS

The authors gratefully acknowledge financial support from NSF and ONR.

- 
- [1] The dimensionless Reynolds number is defined by  $Re=uL/\nu$ , where  $u$  is a velocity,  $L$  is a length scale, and  $\nu$  is the kinematic viscosity of the fluid. It is clear that, since  $\nu \sim 10^{-6}$  for a typical liquid, then on the micrometer scale  $Re \ll 1$ .
  - [2] A. Najafi and R. Golestanian, *Phys. Rev. E* **69**, 062901 (2004).
  - [3] E. Purcell, *Am. J. Phys.* **45**, 3 (1977).
  - [4] H. A. Stone and A. D. T. Samuel, *Phys. Rev. Lett.* **77**, 4102 (1996).
  - [5] J. E. Avron, O. Gat, and O. Kenneth, *Phys. Rev. Lett.* **93**, 186001 (2004).
  - [6] R. Dreyfus, J. Baudry, M. L. Roper, M. Fermigier, H. A. Stone, and J. Bibette, *Nature (London)* **437** 862 (2005).
  - [7] A. S. Mikhailov, *Foundations of Synergetics I. Distributed Active Systems* (Springer, Berlin, 1990).
  - [8] J. D. Murray, *Mathematical Biology* (Springer, Berlin, 1993).
  - [9] A. J. Ijspeert, A. Crespi, D. Ryczko, and J. M. Cabelguen, *Science* **315**, 1416 (2007).
  - [10] I. R. Esptein and J. A. Pojman, *An Introduction to Nonlinear Chemical Dynamics: Oscillations, Waves, Patterns, and Chaos*, Oxford University Press, (Oxford, 1998).
  - [11] M. Shibayama and T. Tanaka, *Adv. Polym. Sci.* **109**, 109 (1993).
  - [12] A. Pikovsky, M. Rosenblum, and J. Kurths, *Synchronization; A Universal Concept in Nonlinear Sciences*, (Cambridge University Press, Cambridge, U.K. 2001).
  - [13] J. Lighthill, *SIAM Rev.* **18**, 161 (1976).
  - [14] It is clear that the frequency must be the same by considering the opposite case. If one part of the snake has some frequency  $f_p$  and a nearby region has frequency  $f_p + \delta$ , then, no matter how small  $\delta$ , given enough time the two regions will get out of phase. When they are out of phase, then they will have drastically different chemical compositions. However, diffusion tends to strongly inhibit sharp spatial variation in concentration, hence preventing this scenario.